PCCP

Accepted Manuscript

ROYAL SOCIETY OF CHEMISTRY

www.rsc.org/pccp

Dynamic action mechanism of small cationic antimicrobial peptides

J.J. Lopez Cascales [†,*], A. Garro[†,‡], R.D. Porasso[§] and R.D. Enriz[†,‡]

July 31, 2014

†Universidad Politécnica de Cartagena, Grupo de Bioinformatica y Macromoleculas (BioMac), Area de Química Física, Aulario II, Campus de Alfonso XIII, 30203 Cartagena, Murcia, Spain
‡Universidad Nacional de San Luis, Facultad de Qumica, Bioquímica y Farmacia, IMIBIO-CONICET, Chacabuco 917, 5700, San Luis, Argentina
§Instituto de Matemática Aplicada San Luis (IMASL) - Departamento de Física, Universidad Nacional de San Luis/CONICET, D5700HHW, San Luis, Argentina.

Abstract

Antimicrobial peptides form part of the immune system as protection against the action of external pathogens. The differences that exist between mammalian and microbial cell membrane architectures is a key aspect in the ability of these peptides to discriminate between pathogen and host cells.

Given that the pathogen membrane is the non-specific target of these cationic peptides, different molecular mechanisms have been suggested to describe the rules that permit them to distinguish between pathogen and mammalian cells. In this context, and setting aside the old fashion idea that cationic peptides act through one mechanism alone, this work will provide insight into the molecular action mechanism of small antimicrobial peptides, based on molecular dynamics simulations of phospholipid bilayers that mimic different cell membrane architectures.

After measuring different properties of these lipid bilayers, in the absence and presence of peptides, a four-step action mechanism was suggested on the basis of the formation of phospholipid rafts induced by the presence of these cationic peptides. Thus, this work shows how differences in the bending constants (k^b) of these lipid rafts and differences in the free energy profiles ($\Delta G(z)$) associated with the insertion of these peptides into these lipid rafts are key aspects for explaining the action mechanism of these cationic peptides at a molecular level.

Keywords:Antibacterial peptides, actuation mechanism, cell membrane, simulation

*To whom correspondence should be addressed: javier.lopez@upct.es

1 Introduction

Antimicrobial peptides (AMP) form part of the innate immune response of all living species against pathogens such as bacteria, funguses and viruses, which have been isolated from vertebrates, insects and plants.[1–5]

Furthermore, it is becoming increasingly clear that cationic antimicrobial peptides have many potential roles in inflammatory responses, orchestrating the mechanisms of innate immunity. Small cationic peptides[6,7] are abundant in nature and have been described as *nature's antibiotics* or *cationic antimicrobial peptides*.

A great number of articles have reported the antibacterial activity of peptides of different molecular size. Some of these peptides show significant antibacterial activity and therefore have drawn the attention of medicinal chemists as potential antibacterial agents, mainly because they are structurally different from current antibacterial agents. However one of the main drawbacks and limitations of these compounds is that so far the molecular mechanism by which these peptides produce their biological effects remains unknown.

In this context, for a proper understanding of the molecular action mechanism of these AMPs, the fundamental differences existing between the microbial and mammalian cells that may represent the target of these peptides must first be specified. Some of these significant distinctions refer to their membrane composition and architecture, which strongly affect their degree of toxicity and selectivity. Most cell membranes are mainly composed of phospholipids and proteins, together with sterols and polysaccha-

rides.[8] However, assuming that this general architecture is applicable to the cell membrane (known as the fluid mosaic model), important differences exist between bacterial and a mammalian cell membranes. Thus, while the outer leaflet of a mammalian cell is mainly composed of zwitterionic lipids (neutral lipids in physiological conditions) and charged lipids are exclusively located in the cytoplasmatic (inner) leaflet of the membrane,[8–10] in the case of pathogen cell membranes, both leaflets of the membrane are enriched with charged phospholipids.[5,9] This different lipid composition between the pathogen and mammalian membrane seems to be crucial for explaining the discrimination mechanism of these AMPs.[5,9,10]

Polypeptides that exert antimicrobial activity have been isolated from different organisms.[11] A striking feature related with antimicrobial peptides is that they are cationic peptides that can form amphipathic structures under certain conditions.[9,10] An essential requirement for any antimicrobial agent is that they must show selectivity. In this regard, these peptides seem to have a selective toxicity for the microbial targets, following a mechanism by which they are capable of distinguishing between microbial and mammalian cells, circumventing their potential toxicity. Hence, electrostatic affinity for the charged pathogen membrane seems to be a key aspect to confer selectivity to these antimicrobial peptides.[10]

Furthermore, a general characteristic of these antimicrobial peptides is that they show an amphipathic nature that matches the cell membrane phospholipid composition, strengthening in this way their interactions with the pathogen cell membrane.[9] Thus, specific structural parameters such as their conformation, charge or amphipathic-

ity need to be taken into consideration for a proper understanding of their activity. Although the sequence of residues that form these peptides varies widely, their secondary structures are almost restrained to $\alpha - helical$ and $\beta - sheet$ structures, being these peptides enriched in lysine, arginine, proline and tryptophan (where lysine and arginine confer the positive charges to the peptide in physiological conditions).[5,9,11] Furthermore, the $\alpha - helical$ conformation of many of these peptides is only adopted in the vicinity of the target membranes.[9,11,12]

As regards the net charge of these peptides, antimicrobial peptides present a net positive charge that ranges from +2 to +9, the peptides showing, in general, well defined cationic domains.[9,11] Thus, the cationic nature of these peptides is of an undoubted importance acting as a driving force toward the pathogen target membrane whose outer leaflet is enriched with negative phospholipid. Despite the good correlation between the number of positive charges of these peptides and their antimicrobial activity, this correlation is not perfect and, in a great number of cases, deviates from linearity. Indeed, there is a charge limit beyond which any increase in the cationic charge does not enhance its antimicrobial activity.[13] Hence, the amphipathicity of these peptides is another critical aspect that must be taken into consideration when we refer to their activity, because this property provides the ability to interact with the hydrocarbon region of the lipid membrane through their hydrophobic side, tending to dissolve into the membrane (disturbing the mechanical properties of the membrane) and affecting its mechanical stability.[9]

On the basis of all the above, and in view of the general consensus existing to-

day about the critical importance of the electrostatic interaction as the driving force of these cationic antimicrobial peptides, the idea that these antimicrobial peptides act on the membrane by means of one unique mechanism is an old fashion argument that has been considered obsolete. However, the existence of some common aspects in all the mechanisms proposed to date confirms the view that the activity of these peptides requires a threshold peptide concentration on the membrane surface to induce the phase transition of the lipids that constitute the membrane.[9,11] Furthermore, once this threshold concentration is achieved on the external leaflet, different peptide quaternary structures have been suggested (and measured experimentally) based on formation of barrel-stave or toroidal shape structures, which could explain their lytic activity.[9,11] The carpet mechanism is another non-specific mechanism in which a threshold peptide concentration is required for lytic activity to occur as a result of the disruption of the physical properties of membranes when peptides are bound to the membrane.[14]

In this context, and with the aim of providing insight into the role played by the membrane composition on the action mechanism of antibacterial peptides, simulations of lipid bilayers with different phospholipid compositions were carried out in the presence and absence of antimicrobial peptide. Thus, the lipid bilayer was modelled using mixes of charged and zwitterionic lipids in different ratios. On this basis, lipid bilayers were assembled, varying from bilayers composed only of zwitterionic DPPC (DipalmitoylPhosPhatidylCholine) lipids to bilayers composed exclusively of charged DPPS (DipalmitoylPhosPhatidylSerine) lipids, passing through binary bilayers formed of DPPC+DPPS in different proportion. All the bilayers were modelled bearing in

mind a symmetric lipid compositions on both leaflets of the membranes. A peptide with a primary structure $RQWRRWWQR-NH_2$ was employed as antibacterial peptide. This is a small synthetic peptide with only 9 aminoacids and a charge of +4, with good antibacterial and antifungal activity.[15] Thus, considering bilayers of different lipid compositions in the presence of variable concentrations of peptides, several molecular dynamic simulations were carried out with the aim of providing insight into the mechanism of action of this small antibacterial peptide. In this sense, an action mechanism for this peptide has been proposed, in line with the previous mechanism proposed by Shai-Matsuzaki-Huang.[14,16,17]

2 Methods and models.

2.1 Simulation parameters.

The engine used for the molecular dynamics simulations was the Gromacs package 4.5.3.[18,19] An integration time step of 2 fs was used in all the simulations. The long range interactions were simulated using the Lennard Jones potential, and the electrostatic interactions were calculated using the Particle Mesh Ewald method.[20,21] In both cases, for the Lennard Jones and electrostatic interactions, a cut-off of 1 nm was used. The charge distributions of DPPS, Na+ and Cl- were halved to compensate for the absence of polarizability in the models used in the simulations, as has been argued in previous works. In this respect, several physicochemical reasons justify this charge reduction, such as it has been discussed elsewhere.[22–26] The molecular bonds were restrained using the Lincs algorithm[27] and the simulations were carried out under NPT

thermodynamic conditions, with a weak temperature and pressure coupling bath algorithm[28] to the temperature and pressure of 310 K and 1 atm, with coupling constants of 0.1 and 1ps for temperature and pressure, respectively. Under these conditions, 100 ns of trajectory length were simulated for different numbers of peptide adsorbed on the surface of the lipid bilayer. All the simulations were carried out at 350 K, a temperature that was chosen because it is above the transition temperature of 314 K[29] and 326 K[30] for pure bilayers of DPPC and DPPS, and also because this temperature is above the transition temperature of all the binary bilayers formed by DPPC/DPPS, as deduced from their experimental phase diagram.[31] In short, the temperature of 350 K ensures that all these binary bilayers are in a liquid crystalline state, which corresponds to the phase of biological significance, regardless of the fraction of DPPS in the lipid bilayer.

Bilayers of different DPPC+DPPS composition were simulated using the force fields described in previous works,[23,25] and the peptide was simulated using the GROMOS 54a7 forcefield.[32] Finally, the single point charge (SPC)[33] was the water model considered in all our simulations.

3 Simulation Results.

3.1 Bilayer bending modulus, k^b.

Five different lipid bilayers were generated in order to analyse the full range of lipid compositions of binary bilayers composed of DPPC and DPPS. The starting system was formed by a bilayer composed of 288 DPPC molecules (144 DPPC per leaflet) and 10068 water molecules of the Single Point Charge (SPC) water model.[33] Once

this bilayer of DPPC had been generated, four additional bilayers were constructed by substituting 48, 96,192 and 288 DPPC molecules by 48, 96, 192 and 288 DPPS molecules. To balance the negative charge associated with each DPPS molecule under physiological conditions, 48, 96, 192 and 288 sodium ions (Na^+) were introduced into the system, substituting water molecules by sodium ions. In summary, five different binary bilayers of DPPC:DPPS were generated with the following compositions 288:0, 240:48, 192:96, 96:192 and 0:288.

The molecular fraction of DPPS that forms the lipid bilayer, χ, was defined as follows:

$$\chi = \frac{n_{DPPS}}{n_{DPPC} + n_{DPPS}} \tag{1}$$

where χ represents the molecular fraction of DPPS with respect to the total number of lipids in the bilayer.

To simulate an 0.5 M NaCl aqueous solution, two water molecules were randomly substituted by one sodium and one chloride ion, respectively, every 28 water molecules in each of the systems generated above.

The bilayer bending modulus, k^b, in a lipid bilayer can be calculated as follows;[34]

$$k^b = \frac{K_A \xi^2}{24} \tag{2}$$

where, ξ is defined as the *effective* thickness of the lipid bilayer, with $\xi = d_{HH} - 1$ in nm and d_{HH} is the distance between the maximum of the head density distribution in both leaflets of the lipid bilayers (in our case, we considered the peaks of the phospho-

without NaCl				
χ	Area/nm^2	$\frac{d_{HH}}{2}/(nm)$	$K_A/(N/m)$	$k^b/(k_BT)$
0.0	0.683± 0.007	1.5	0.468±0.005	16.4±0.2
0.17	0.626± 0.007	1.59	0.429±0.005	17.4±0.2
0.33	0.586± 0.007	1.83	0.401±0.008	17.2±0.2
0.67	0.531± 0.006	2.08	0.424±0.005	24.9±0.3
1.0	0.533±0.006	1.76	0.426±0.005	31.8±0.4
with 0.5 M NaCl				
0.0	0.676± 0.008	1.52	0.406±0.005	15.84±0.08
0.17	0.620± 0.007	1.64	0.425±0.005	18.5±0.2
0.33	0.577± 0.006	1.87	0.461±0.006	22.1±0.2
0.67	0.520± 0.006	2.05	0.416±0.005	26.5±0.3
1.0	0.526±0.005	1.79	0.504±0.005	36.3±0.4

Table 1: Surface area per lipid, compressibility modulus (K_A) and bending modulus (k^b), as a function of the molecular fraction in DPPS in the lipid bilayer, χ. The error bars were calculated from the last three subtrajectories of 30 ns each, where the first 10 ns were discarded as being the equilibration time.

rus atom distributions in both leaflets of the bilayer). K_A represents the compressibility modulus, which is defined as follows,

$$K_A = \frac{k_B T A}{\sigma^2(A)} \tag{3}$$

where, A and $\sigma^2(A)$ correspond to the mean and mean-squared fluctuation of the interfacial area, respectively, k_B is the Boltzmann constant, and T, the temperature.

Table 1 shows the k^b values obtained for all the bilayers studied, in the absence and presence of salt. For the DPPC bilayer (without DPPS), corresponding to $\chi = 0$, values of $16.4 \pm 0.2\ k_BT$ and $15.84 \pm 0.08\ k_BT$ were obtained for k^b in the absence and presence of salt, respectively. These values are in good agreement with the experimental data of 16.7 k_BT obtained from X-ray measurements[35] of DMPC lipid bilayers in their liquid crystalline phase and from pipette aspiration measurements, which were in a range of 11 to 30 k_BT, depending on the length of the lipid hydrocarbon tails of

PC-phospholipids[36,37] and 15.8 k_BT for a DOPC bilayer with unsaturation in its lipid chains.[38] They also agree with the measurements from Neutron Spin Echo experiments (NSE), where a value of 25.5 k_BT[39] was obtained, the difference between these and our results possible being due to the different temperatures at which the experiments and simulations were performed because of the temperature dependence of the bending modulus.[39]

For the k^b of a bilayer of DPPS, values of 31.8±0.4 and 36.3±0.4 k_BT were estimated by simulation in the absence and presence of salt. These values are in a reasonably good agreement with the value of k^b provided by Petrache et al.[40] from high resolution x-ray measurements, where a value of 26 k_BT was estimated for a DOPS bilayer. The slight difference between simulation and experimental data may be related with the increase in elasticity of lipid bilayers with the unsaturation of the lipid chains, as Rawicz et al[37] proposed based on pipette aspiration measurements.

From the values of Table 1, it can be seen how the bending modulus increases with the fraction of DPPS in the bilayer, χ, in both the absence and presence of salt. From this behaviour it is deduced that the presence of salt in the solution enhances the bending modulus of the lipid bilayer, this difference in k^b increasing with the molar fraction of DPPS in the lipid bilayer.

From the behaviour of k^b with χ, and given that K_A remains almost constant for the whole range of molecular fractions of DPPS that form the bilayer (see Table 1), the influence of the thickness of the lipid bilayer on its elastic properties should be noted.

The effect of the ionic strength on the bending rigidity agrees closely with the

experimental data provided by Claessens et al.[41] for a DOPG and DOPC bilayer at different ionic strengths of the aqueous solution. Thus, these authors determined how the bending modulus of charged bilayers formed by DOPG is higher than the corresponding one formed only by DOPC. Furthermore, the bending modulus of charged bilayers of DOPG also increases with the ionic strength of the aqueous solution, behaviour that is in a perfect agreement with the results from our simulations.

3.2 Peptide-bilayer interactions.

3.2.1 Assembling the systems.

Three periodical boxes were generated for the different types of lipid bilayers studied in this work, as follows:

1. DPPC bilayer: This lipid bilayer was formed with 648 DPPC distributed on both symmetric leaflets (324 DPPC on each), with $\chi = 0$, and 28526 water molecules.

2. DPPC+DPPS bilayer: This lipid bilayer was formed with 108 DPPS + 540 DPPC, 108 Na^+ and 27878 water molecules, corresponding to $\chi = 0.17$.

3. DPPS bilayer: This bilayer was generated by substituting 648 DPPC molecules of case 1 by 648 DPPS, while 648 sodium ions were introduced into the system to balance the charge by random substitution of a water molecule by sodium ion, which reduced the total number of water molecules to 27980 water molecules, corresponding to $\chi = 1$.

Once the three lipid bilayers were generated and their conformational parameters stabilized, different number of peptides were inserted into these systems on one of the

two sides of the membrane. Thus, in the DPPC and DPPC+DPPS bilayers, 10, 20 and 40 peptides were introduced into the system. In the case of the DPPS bilayer, only the case with 40 peptides was simulated. In order to investigate the effect of ionic strength, a 0.5 M NaCl aqueous solution was simulated.

Finally, it should be mentioned that at the beginning of our simulations peptides were randomly positioned in bulk water on one side of the phospholipid bilayer. Next, they were then brought into the vicinity of the lipid bilayers by a harmonic biasing potential applied to the centre of mass of each peptide to reduce expensive computational time. Once they were close enough to the lipid bilayers, the biasing potential ceased, and the peptides recovered their freedom of motion. In this regard, Figure 1 shows a snapshot of the DPPC lipid bilayer with 40 peptides adsorbed on the external leaflet.

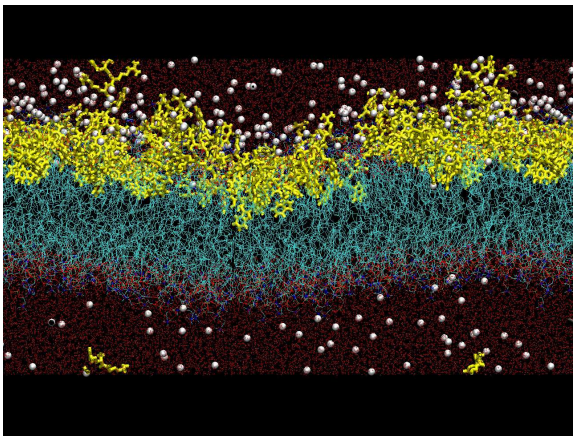

Figure 1: Snapshot of the DPPC bilayer with 40 peptides adsorbed on the external leaflet, and chloride ions to balance the positive charge of the antimicrobial peptides.

3.2.2 Surface area per lipid and bilayer thickness in presence of AMPs.

To illustrate the perturbing effect of AMPs adsorbed on the outer leaflet of a phospholipid bilayer, we will express the peptide concentration adsorbed on the external leaflet as a function of the ratio between the peptide adsorbed and phospholipid of the leaflet (P/L). In a first instance, Figure 2 shows the temporal evolution of the surface area per DPPC lipid in absence of peptides (P/L=0/324). With the aim of confirming the stability of the simulated system, Figure 2 shows the running surface area per DPPC molecule in the absence and presence of peptides adsorbed on the phospholipid bilayer at a ratio of P/L=1/16. From this figure, we observe how for both cases, the surface area per lipid achieves a stationary state after 10 ns of simulation time.

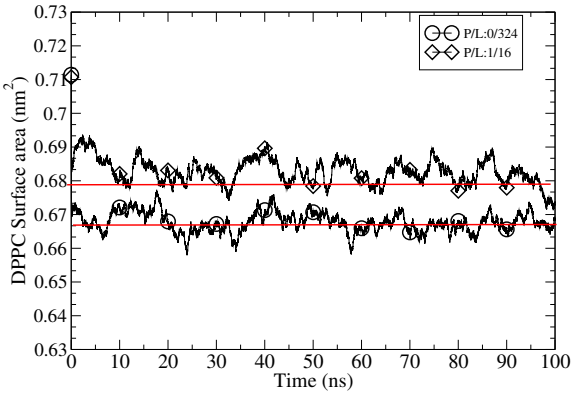

Figure 2: Running surface area per lipid in the presence and the absence of AMP.

For the system with a peptide/lipid ratio (P/L) of 1/8, the trajectory was extended for additional 100 ns of simulation, because the system did not reach an equilibrated state before reaching 75 ns of simulation time.

P/L ratio	Bilayer DPPC (nm^2) $\chi = 0$	Bilayer DPPC+DPPS (nm^2) $\chi = 0.17$	Bilayer DPPS (nm^2) $\chi = 1$
0	0.667 ± 0.003	0.602 ± 0.003	0.5439 ± 0.0009
1/32	0.673 ± 0.003	0.609 ± 0.004	–
1/16	0.682 ± 0.003	0.6079 ± 0.0014	–
1/8	0.719 ± 0.006	0.62 ± 0.03	–
1/8 *	0.689 ± 0.004	—	–

Table 2: Surface area per phospholipid for the three models of lipid bilayers studied at different concentrations of peptide adsorbed on the external leaflet (expressed as Peptide/Lipid ratio) of the lipid bilayer. Value labelled 1/8* correspond to the surface area in presence of 0.5 M NaCl aqueous solution.

Thus, discarding the first 10 ns of the trajectory length in all cases except for P/L=1/8, Table 2 shows the surface are per DPPC molecule as a function of the peptide concentration adsorbed on the lipid bilayer.

Table 2 shows how in the absence of NaCl in solution, an increase in the peptide concentration adsorbed on the phospholipid bilayer produced an expansion of the external leaflet of the DPPC bilayer. However, in the presence of NaCl in the water solution, this membrane swelling (due to the presence of peptide) is compensated by the natural shrinking in the surface area per lipid associated to the presence of NaCl in solution.[42–44] Hence, since both effects (bilayer expansion associated to the presence of peptides and the shrinkage associated to the presence of NaCl in solution) tend to cancel each other, the result is that the bilayer remains almost unperturbed in presence of salt even for high ratios of peptide adsorbed on its leaflets.

An important effect associated with the expansion of the phospholipid surface (due to the adsorption of peptides) is the decrease in the bilayer thickness. Thus, Figure 3a shows the atomic density distribution of phosphorus atoms of DPPC for both leaflets of the lipid bilayer. Considering the bilayer thickness as the distance from the phosphorus

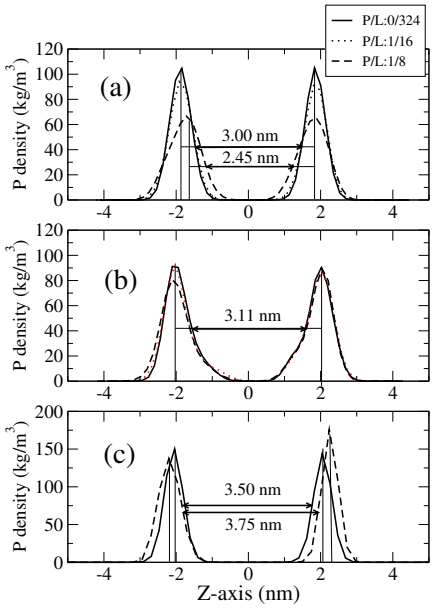

Figure 3: Thickness of the lipid bilayers in presence and absence of peptide adsorbed. (a) DPPC bilayer, (b) DPPC+DPPS bilayer and (c) DPPS bilayer. Thickness was estimated considering the distance of the phosphorus mass distribution for both leaflets of the lipid bilayer measured at the half height of the peak of the phosphorus distributions.

distribution at half height of both peaks, as expressed in Figure 3.a, a constant value of 3 nm is obtained for the thickness of the lipid bilayer, even for P/L ratios as high as P/L=1/16. However, at P/L=1/8 there is a noticeable diminution in the thickness of the lipid bilayer, which falls to 2.45 nm, a reduction of roughly 20 % with respect to the bilayer in the absence of peptide. In the presence of 0.5 M NaCl, for a P/L of 1/8, a thickness of 3.0 nm was measured which is in line with the value measured for the DPPC bilayer in the absence of peptide.

In summary, Figure 3a shows how the presence of peptide adsorbed on the lipid bilayer produces a significant perturbation in the structure of a DPPC bilayer when

the peptide adsorbed on the lipid bilayer reaches a certain threshold concentration, at which an expansion of the surface area per lipid and a reduction in the thickness of the bilayer become evident.

This behaviour contrasts with that observed in binary DPPC+DPPS bilayers. Table 2 and Figure 3b show that the surface area per lipid and the thickness of the lipid bilayer remained unperturbed for the whole range of P/L studied.

Finally, for the case of a bilayer composed exclusively of DPPS and for the highest P/L ratio studied in this work (corresponding to P/L=1/8). Figure 3c, the lipid bilayer shrinks with a consequent increase of roughly 7% in the thickness of lipid bilayer.

Thus from the results depicted above, we observe how an increase in the DPPS content in the lipid bilayer reduces the expansion of the surface area per lipid and minimizes the reduction in the thickness of the lipid bilayer, for high concentrations of peptide adsorbed on the lipid bilayer. Although this perturbing effect is most noticeable in the DPPC bilayers, it almost disappears for concentrations of 0.5 M NaCl in aqueous solution, as is shown in Table 2.

3.2.3 Order parameters, $-S_{CD}$.

The deuterium order parameters of aliphatic chains provide valuable information about the structure and disorder in the interior of the lipid bilayer. Experimentally, the order parameters of given deuterated methylene groups can be measured using the H-NMR technique.[45,46] From simulation, $-S_{CD}$ can be calculated from the following tensor:

$$S_{\alpha\vartheta} = \frac{< 3cos\vartheta_\alpha cos\vartheta_\beta - \delta_{\alpha\beta} >}{2} \quad \alpha = x,y,z; \beta = x,y,z \tag{4}$$

where ϑ is the angle between the molecular axis, i, and the perpendicular direction to the bilayer plane, and $\delta_{\alpha\beta}$ is the Kronecker's delta. Thus, the molecular axes are defined as follows:

1. The Z-axis is a vector that connect the carbons of the methylene groups, C_{i-1} and C_{i+1}.

2. The X-axis is a vector perpendicular to the Z-axis that is contained in the plane defined by the carbons of the methylene groups C_{i-1} and C_{i+1}.

3. The Y axis is a vector normal to the other two axe, X and Z.

From simulation, $-S_{CD}$ can be estimated from the tensor $S_{i,j}$ defined above, as follows:[25,47]

$$-S_{CD} = \frac{2S_{xx}}{3} + \frac{S_{yy}}{3} \tag{5}$$

.

Figure 4 shows the order parameters for the three models of lipid bilayer studied in this work, in the absence and presence of peptides adsorbed on the bilayer surface. From this figure, it can be seen how the DPPC bilayer in the presence of peptide remains almost unperturbed until a critical concentration is achieved. However, the presence of salt in the aqueous solution inhibits the effects associated to the presence of peptides adsorbed on the surface, even for peptide/lipid ratios above the critical value determined in the absence of salt.

A binary bilayer composed of DPPC+DPPS with a $\chi = 0.17$, behaves similarly to

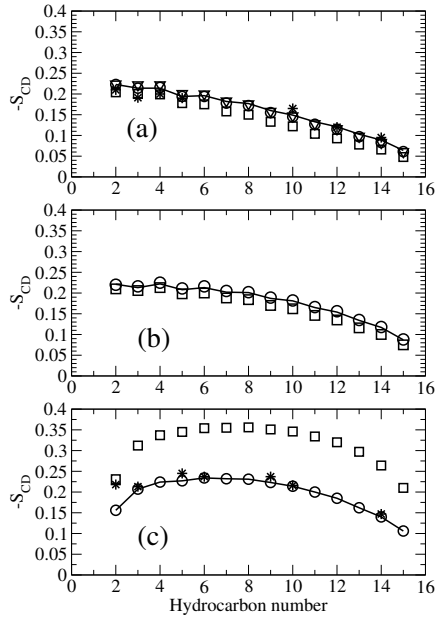

Figure 4: Deuterium order parameters corresponding to the three type o lipid bilayers studied in this work. (a) DPPC bilayer, (b) DPPC+DPPS bilayer and (c) DPPS bilayer. (*) Experimental data in absence of peptide, (−) simulated data without peptide, (○) simulation data corresponding to a peptide/lipid ratio of 1/16, (□) simulation data corresponding to a peptide/lipid ratio of 1/8 and (▽) simulation data corresponding to a ratio of peptide/lipid of 1/8 in a 0.5 M NaCl in aqueous solution.

a DPPC bilayer, although ii is less sensitive to the presence of peptides adsorbed on the surface, for the whole range of P/L studied.

Finally, in the case of the DPPS bilayer, there is an increase in the order parameters for P/L=1/8, which suggests that in the presence of peptides at P/L ratios above a certain critical value, a phase transition from liquid crystalline to gel is induced in the lipids that form the lipid bilayer.

3.2.4 Bilayer Lateral pressure, $\pi(z)$.

The lateral pressure profile across a lipid bilayer, $\pi(z)$, is a key aspect related with its mechanical stability. A characteristic of $\pi(z)$ is that it is non-uniform across the lipid bilayer, as a consequence of the inhomogeneous molecular interactions that take place between neighbouring lipids and between lipids and the aqueous solution. Computationally, the lateral pressure profile can be estimated using the Lindhal and Edholm algorithm.[48] Thus, the lateral pressure profile along the Z-axis perpendicular to the bilayer plane, $\pi(z)$, can be calculated as follows,

$$P = \sum_{i \in slice} m_i v_i \otimes v_i - \frac{1}{\Delta V} \sum_{i<j} F_{ij} \otimes r_{ij} f(z, z_i, z_j) \tag{6}$$

where the first term of the above summatory corresponds to the kinetic contribution from all the particles that fall in the i-slice, ΔV is the volume associated with each slice of Δz thickness, and $f(z, z_i, z_j)$ corresponds to a discrete function defined as follows:

1. If both particles fall in the same slice, *i*, $f = 1$.
2. If both particles are outside slice *i* and on opposite sides, $f = \frac{\Delta z}{|z_i - z_j|}$.
3. If one particle is in slice *i* and the other outside, $f = \frac{\Delta z}{2|z_i - z_j|}$

In this regard, Figure 5 shows the lateral pressure profile for the DPPC bilayer in the absence and presence of different concentrations of peptide adsorbed on the external leaflet of the membrane. Figure 5a shows how, from a qualitative point of view, the pressure profile $\pi(z)$ reproduces almost the same $\pi(z)$ profile, up to P/L ratios of 1/16.

Furthermore, we observe how the difference in pressure between the first minimum and the maximum located in the middle of the phospholipid bilayer increases with the P/L ratio of peptides adsorbed on the membrane. This divergence in the pressure profile is clear evidence of the increased instability of the lipid bilayer in the presence of peptide adsorbed on the membrane surface, while the pressure profile for the leaflet remains almost invariable in the absence of peptide for the whole range of P/L studied.

However, when the ratio P/L reaches a certain critical value, that we estimate to be of P/L=1/8, the pressure profile completely loses its original shape (see Figure 5b) illustrating how the molecular symmetry is lost across the lipid bilayer. This shape of the $\pi(z)$ profile could correspond to an incipient state of the lipid bilayer that ends with the collapse of the bilayer structure.

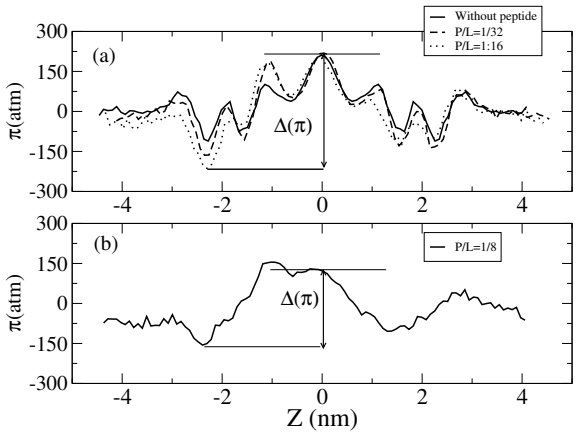

Figure 5: Lateral pressure profile $\pi(z)$ of a DPPC bilayer for different concentrations of peptide adsorbed on the external leaflet of the lipid bilayer.

For the case of binary bilayers formed of DPPC+DPPS, Figure 6 shows how the lateral pressure $\pi(z)$ maintains the same profile (from a qualitative point of view) for the

whole range of peptides adsorbed on the external leaflet of the lipid bilayer, confirming the great stability of this bilayer in the face of the perturbing effect associated to the presence of these peptides adsorbed on the bilayer surface.

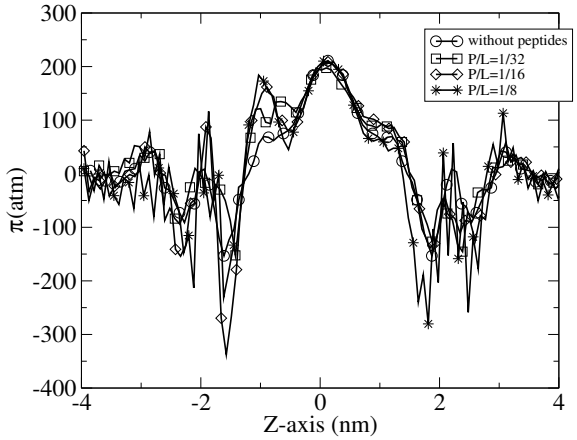

Figure 6: Lateral pressure profile $\pi(z)$ of a DPPC+DPPS bilayer, for different concentrations of peptide adsorbed on the external leaflet of the lipid bilayer.

Finally, for the DPPS bilayer (figure not included), peptides adsorbed on the external leaflet produced a very slight perturbing effect on the lateral pressure profile, $\pi(z)$, even for the highest ratio of P/L=1/8 adsorbed on the lipid bilayer.

3.2.5 Thermodynamics of peptide insertion into lipid bilayers.

The partition function of a given specie between two different mediums is directly related with the difference of free energy (ΔG) associated with this process, as follows:

$$\Delta G(z) = -RT \ln \frac{C(z)}{C^*} \tag{7}$$

where, $C(z)$ corresponds to the specie concentration at a certain position z per-

pendicular to the interface, and C^* its concentration in bulk solution. In our case, we explore the difference of free energy associated with the peptide insertion into a DPPC bilayer (with $\chi = 0$) and a bilayer formed by DPPC+DPPS (with $\chi = 0.17$).

To estimate the difference of free energy associated with the insertion of our antimicrobial peptide into a lipid bilayer, the Umbrella[49] and WHAM[50] methods are followed because $C_{peptide}(z)$ can not be accurately determined during the simulated trajectories due to the poor sampling of the configurational space during the simulation time.

In our case, two new computational systems were generated. The first was composed of 288 DPPC (144 per leaflet), 17516 water molecules of the SPC model and the corresponding Cl^- to balance the charges of the system, while the second one was composed of 240 DPPC and 48 DPPS (120 DPPC+ 24 DPPS per leaflet), 15430 water molecules of the SPC model, and Na^+ and Cl^- to balance all the charges of the system. In each of these two new models of lipid bilayers, two peptides were positioned far from each other with the aim of avoiding unwanted interactions of each other. Thus, one of the two peptides was positioned in the bulk water (Z = -4 nm) and other one in the core of the hydrocarbon region of the lipid bilayer (Z = 0 nm). The motion of both peptides along the Z-axis perpendicular to the bilayer surface was restrained by application of a Hookean potential to their centre of mass, such that their motion was restrained along the Z-axis, but they maintained their freedom in the X-Y bilayer plane. From the starting conformation, the peptides were shifted from Z= -4nm to Z= 4nm in 0.1 nm steps, while maintaining the distance between them at a constant 4 nm. In this

way, a total of 41 windows were generated. Following the Umbrella[49] and WHAM[50] methods, the free energy profile associated to the insertion of these peptides into the above mentioned lipid bilayers was estimated.

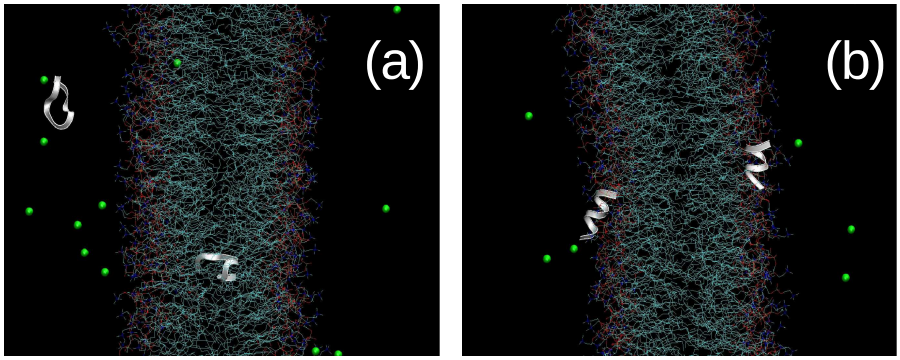

Figure 7: Two snapshots corresponding to two windows used in the calculation of the ΔG associated to the insertion of peptide into a DPPC bilayer.

Figure 7 shows two snapshot corresponding to two of the windows used for the calculation of the free energy profiles. Figure 8 shows the free energy profile $\Delta G(z)$ associated to peptide insertion into a DPPC and into a binary DPPC+DPPS bilayer, respectively. From Figure 7, it is deduced how the adsorption of peptides is a spontaneous process regardless of the bilayer composition, although this process is much more favourable in the case of a DPPC bilayer than in the case of a binary bilayer with a high DPPS content. In addition, Figure 8 shows how the minimum in the DPPC bilayer

is shifted toward the deepest zones of the bilayer, contributing in a certain manner, to the destabilization of the lipid bilayer.

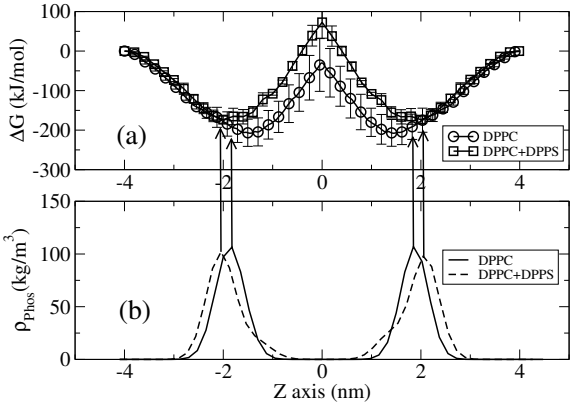

Figure 8: (a) Free energy profile $\Delta G(z)$ related with the insertion of peptide into a DPPC and DPPC+DPPS bilayer with $\chi_{DPPS} = 0.17$.(b) Phosphorus density across the Z axis in both membranes.

Hence, this displacement of the minimum of $\Delta G(z)$ toward the deepest zones of the aliphatic region of the DPPC bilayer (unlike in the binary DPPC+DPPS bilayer where the minimum is located at the lipid head region) has two major effects on the DPPC bilayer stability:

1. In the DPPC bilayer, peptides adsorbed on the external leaflet are able to interact with the lipid heads of the opposite leaflet. Thus, Figure 9b shows how for the case corresponding to the binary DPPC+DPPS bilayer and a ratio of P/L=1/8, the peptide atom distribution is almost centred with respect to the phosphorus distribution in the phospholipid heads on which they were adsorbed. On the contrary, in the case of the DPPC bilayer, Figure 9a shows how the distribution of peptide atoms extends until they overlap the distribution of phosphorus in the

opposite leaflet.

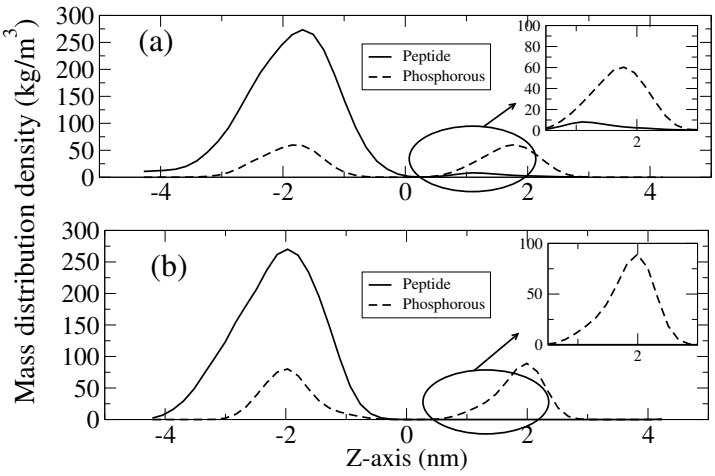

Figure 9: Mass density distribution of peptide and phosphorus of the lipid bilayer. (a) DPPC bilayer and (b) DPPC+DPPS .

2. The much deeper intrusion of the peptide into the DPPC bilayer than to the binary DPPC+DPPS bilayer, and the lower curvature module k^b of the DPPC bilayer (much greater flexibility than in DPPC+DPPS, Table 1) suggest that DPPC bilayers will become much more unstable in the face of peptide adsorption than DPPS enriched bilayers.

4 Discussion.

Section 3.1 shows how the curvature module, k^b, in lipid bilayer increases with the fraction of charged lipids of the lipid bilayer. This means that phospholipid bilayers enriched in charged phospholipids are more rigid, planar and mechanically stable than bilayers poor in charged phospholipids, behaviour which is enhanced with an increase in the ionic strength of the aqueous solution.

In this context, most of the action mechanisms of antimicrobial peptides proposed so far have exclusively been focused on the primary, secondary and quaternary structure of peptides and the charged nature of the pathogen membrane. However, little thought have been given to the possibility of the formation of transitory lipid rafts in the external leaflet of the membrane cell, which, eventually, could perturb the mechanical properties of the membrane induced by the electrostatic interaction with the peptides adsorbed on the membrane cell.[51,52] In the case of the host cell, and due to the fact that the external membrane leaflet is mainly composed of zwitterionic lipids (without a net charge), antimicrobial peptides are poorly attracted to the membrane surface because of the weak electrostatic attraction, and hence, membrane-peptide electrostatic interactions do not play a relevant role in this process. In this regard, the possibility that peptides could reach a critical concentration on the membrane surface is very slight, and so, they will not become toxic, in line with most of the mechanisms proposed so far.[5,9,10,14,53]

In contrast, the existence of charged phospholipids in the external leaflet of the pathogen membrane, induces the adsorption of these peptides to the membrane, mediated by electrostatic interactions between the net negative charge of the membrane and the positive charge of the antimicrobial peptide. As these peptides leave the bulk solution and approach the vicinity of the lipid bilayer, or even after they have been anchored to the membrane surface,[9,10,14] they fold into an $\alpha - helix$ conformation (induced by the variation of the dielectric constant of the environment, as has been described elsewhere[12,15]). In line with this, Figure 7 shows how 30 ns of simulation time is sufficient for the peptide in bulk solution and at middle of the lipid bilayer to unfold, compared

with the behaviour shown by the peptides at the lipid/water interface in which they maintain their $\alpha - helical$ conformation.

Hence, our action mechanism suggests that as the peptide approaches to the lipid bilayer, and as a consequence of strong electrostatic interactions between the peptides and charged lipids located in the external leaflet, the formation of lipid domains of different compositions is induced in the membrane . As a consequence of this emergence of lipid rafts, the mechanical properties of the membrane vary (in terms of the curvature module, k^b). Thus, k^b increases with the fraction of charged phospholipids in the membrane (or in other words, the presence of charged lipids increases the stiffness of the membrane) in accordance with the values of Table 1. In this context, the segregation of phospholipids to generate lipid rafts mediated by electrostatic interactions between AMPs and charged phospholipids is a critical step for explaining the molecular activity of these peptides, based on emerging mechanical inhomogeneities along the frontier lines that separates lipid domains in the membrane.

In this context, assuming that the simulated cell membrane presents (in the initial state) a homogeneous lipid composition in its external leaflet that mimics the phospholipid composition of a pathogen cell membrane with curvature module k_0^b, the formation of lipid rafts in the membrane enriched in charged phospholipids leads that the curvature module of the membrane to adopt new values, with $k_1^b > k_0^b$. As a consequence, an increase in the stiffness of this membrane patch is to be expected. On the other hand, due to the fact that the formation of domains rich in charged phospholipids involves the emergence of other lipid domains poor in charged phospholipids (since the

total number of lipids remain constant along this segregation process), a new curvature constant, k_2^b, below the starting value of k_0^b is also to be expected ($k_2^b < k_0^b$), with the consequent enhancement of its flexibility (in line with the values obtained in Table 1). These differences in the mechanical properties of the membrane which are associated to the existence of lipid domains mediated by charged peptides on the pathogen membrane, could be a crucial step for their molecular activity. Furthermore, our simulations showed how, for concentrations of peptide adsorbed on a membranes that mimic the lipid compositions of a pathogen cell membrane (even for peptide-lipid ratios as high as P/L=1/8) the membrane maintained its integrity due to the absence of inhomogeneities in the membrane, with a curvature module k_0^b. This result is borne out by the analysis of different properties of the lipid bilayer, such as the lateral pressure profile $\pi(z)$, order parameters ($-S_{CD}$), molecular surface area per lipid and thickness of the lipid bilayer, compared with those obtained for bilayers with a low charged phospholipid content.

If we look at the thermodynamic aspects associated with the insertion of this peptide into a lipid bilayer, it is clear how the insertion of these small peptides into the membrane is considerably favoured in leaflets rich in zwitterionic phospholipids rather than in lipid bilayers rich in charged phospholipids. Figure 9 remarks the ability of peptides to penetrate into bilayers poor in charged phospholipids until they interact with phospholipid heads of the opposite leaflet. In this way, they put at risk the integrity of the membrane when they eventually achieve a critical concentration on the membrane surface. In contrast, Figure 9 shows how, for domains rich in charged phospholipids, the peptides remained parallel and anchored to the surface of the membrane, almost

without perturbing the original membrane structure.

Finally, for bilayers constituted only by charged phospholipids ($\chi = 1$), the enhanced stiffness (with $k_1^b >> k_0^b$,) and stability for P/L ratios as high as P/L=1/8, lead to a lipid phase transition from a liquid crystalline phase to a gel one (measured after analysing the deuterium order parameters, $-S_{CD}$, together with the reduction in the surface area per lipid), without disrupting the bilayer integrity.

As regards the effect of the ionic strength on the activity of these AMPs, it was concluded that any increase in the ionic strength diminishes the activity of these antimicrobial peptides, in which almost no variation in the structural properties of the membrane were measured with respect the original properties of the lipid bilayer for the full range of P/L studied. The main physico-chemical reasons that justify this statement are the following:

1. An increase in the ionic strength increases the screening of the electrostatic interactions between peptide and the external leaflet of the membrane, reducing their electrostatic interactions.

2. As Table 1 shows, the presence of salt in water solution increases the stability and stiffness of the lipid bilayer, since k^b increases with the ionic strength of the membrane for all the bilayers studied, reducing the chance of membrane collapse, i.e. the possibility of pore forming in the membrane.

These results agree with experimental data that show that the activity of antimicrobial peptides diminishes or even ceases completely as the ionic strength of the aqueous

solution increases.[54–57]

4.1 Action mechanism of small cationic peptides.

An analysis of all the results discussed in previous sections provides insight into a possible action mechanism for these cationic peptides at a molecular level. In this regard, and on the basis of the properties discussed above, a four step molecular mechanism can be suggested, as summarized in Figure 10.

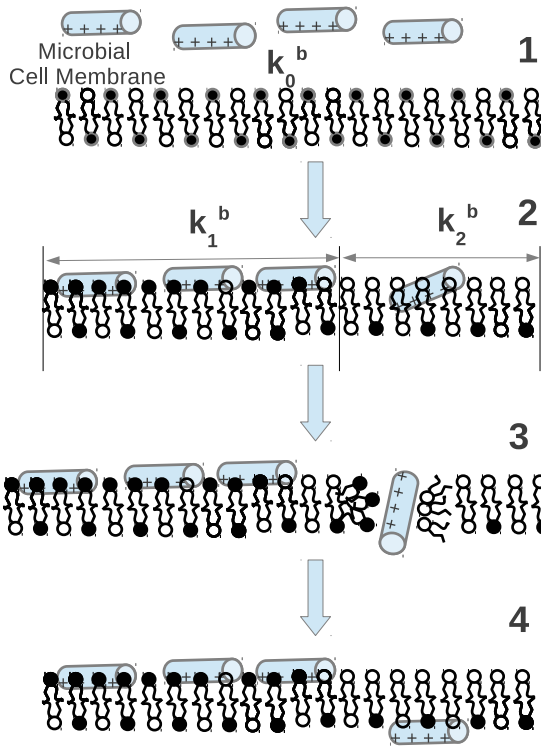

Figure 10: Action mechanism of cationic peptides. • represents DPPS and ○ represents DPPC molecules.

4.1.1 Peptide folding and induction of phospholipid segregation.

Several authors have suggested that antimicrobial peptides possess a random-coil conformation in a water solution, but, when they approach the bilayer/solution interface, they fold into a $\alpha - helix$ conformation.[9,11,12] In this regard, experimental and computational studies showed that these peptides present a random conformation in the bulk solution and that they adopt an $\alpha - helical$ conformation when they are in an environment with a low dielectric constant. A first consequence of peptide folding is the change in its amphipathicity, favouring its electrostatic interaction with the external leaflet of the cell membrane rich in charged phospholipids.[14,53,58]

Unlikely, phospholipid segregation in the cell membrane induced by $\alpha - helical$ peptides falls far away from the order of magnitude accessible to MD simulations. However, the results reported in this work support the idea that this is a key step in the action mechanism of these antimicrobial peptides, as is discussed below:

1. The existence of strong electrostatic interactions between these charged peptides and charged phospholipids located in the external leaflet of the cell membrane suggests that these strong interactions can trigger the formation of lipid aggregations in the membrane.

2. Peptides adsorbed on the bilayer surface do not protrude into lipid bilayers with a high proportion of charged phospholipids (as depicted in Figures 8 and 9).

3. An increase in the proportion of charged lipids in the bilayer composition produces an increase of the curvature module, k^b, enhancing the mechanical stability

of the membrane as well (Table 1).

Thus, on the one hand, the formation of lipid aggregates (or lipid rafts) in the membrane induces inhomogeneities in the curvature modulus of the membrane, k^b, which cab be disrupted due to the abrupt variation of k^b along the frontier lines between neighbouring phospholipid rafts.

4.1.2 Peptide protruding into domains with poor charged phospholipid content.

From a thermodynamic point of view, the insertion of peptides is favoured in bilayers poor in charged phospholipids, as discussed above.

Figure 11a represents a lipid bilayer that mimics the pathogen membrane (with $\chi = 0.17$) and Figures 11b and 11c show two bilayers that resemble domains on the membrane surface induced by the peptides adsorbed on the lipid bilayer, corresponding to $\chi = 1$ (a bilayer formed only by DPPS) and $\chi = 0$ (a bilayer formed only by DPPC), respectively.

Figure 11a shows how peptides are strongly anchored to the membrane at the lipid/water interface. Considering that the curvature modulus of a bilayer with $\chi = 0.17$ is $k_0^b = 17.4 \pm 0.2 k_B T$ (see Table 3.1), and considering the free energy profile of $\Delta G(z)$ associated with peptide insertion into this membrane, peptides adsorbed on the membrane do not drastically perturb the structure of the lipid bilayer, even at high P/L ratios of peptides adsorbed on the membrane. With an increased fraction of DPPS in the membrane, i.e. high values of χ, an increase in the rigidity of the membrane is expected (see Table 1). As a consequence of this almost 80% increase in k^b with respect

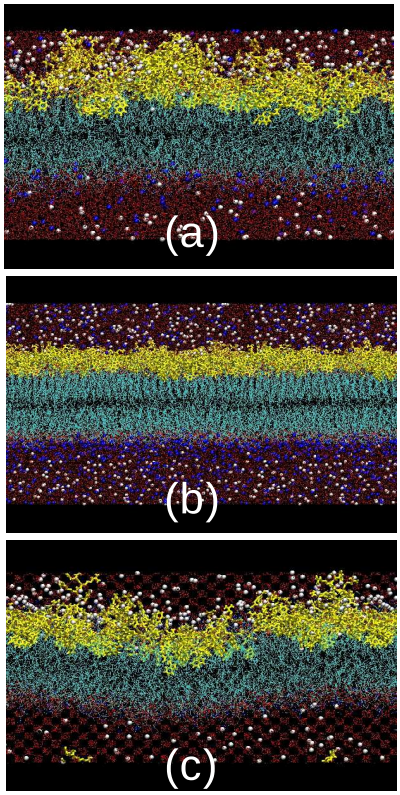

Figure 11: Snapshots of the lipid bilayer with a Peptide/phospholipid ratio of P/L=1/8: (a) corresponds to the initial bilayer that mimic a pathogen membrane with $\chi = 0.17$, (b) membrane formed only by DPPS, with $\chi = 1$. and (c) bilayer in the absence of DPPS, with $\chi = 0$.

to its original value the lipid bilayer becomes much more rigid, flat and stable than the original bilayer of $\chi = 0.17$, removing any chance of membrane collapse, as can be seen in Figure 11b.

Finally, in domains with a poor content in DPPS, represented by $\chi = 0$, values of k^b below the value of the lipid bilayer that mimic a pathogen membrane (k_0^b) can be expected (see Table 3.1). In this case the bilayers are much more waved, flexible and unstable than the bilayers that resemble a pathogen membrane, see Figure 11c.

4.1.3 Membrane collapse and pore formation.

The phospholipid segregation induced by the electrostatic interaction between peptide and charged phospholipid has as a first consequence the emergence of phospholipid patches in the membrane with different bending module, k^b.

Due to the emerging mechanical inhomogeneities in the membrane associated to patches of different lipid composition and the differing free energy profile, $\Delta G(z)$ associated to the insertion of peptides into lipid bilayers of different composition, where $|\Delta G(z)(\chi = 0)| > |\Delta G(z)(\chi = 0.17)|$ the spontaneity associated with the insertion of the peptide into a lipid bilayer diminishes (in absolute values) with the increase in charged phospholipids in its composition, while the minimum of the free energy profile is displaced toward positions occupied by the lipid heads at the bilayer surface.

From an analysis of the properties studied in this work, such as the lateral pressure, surface area per lipid or thickness of the lipid bilayer, it is observed that all the bilayers studied are stable at low concentrations of peptide adsorbed on the membrane. Only in the case of the DPPC bilayer was determined the existence of a threshold peptide concentration, at which the lipid bilayer is disrupted, inducing the membrane collapse.

4.1.4 Peptide transposition and recovering of the bilayer structure.

As the peptide concentration adsorbed on the external leaflet diminishes (due to peptides migration to the inner side of the membrane), the P/L ratio falls to values below its threshold concentration. Under these circumstances and at this instant, the membrane is capable of recovering its original architecture and the lytic activity of these peptides

ceases totally.

5 Conclusions

An action mechanism for small cationic peptides with antimicrobial and antifungal activity is proposed based on the basis of the study of different mechanical and thermodynamic properties of binary lipid bilayers of DPPC+DPPS.

Assuming that peptide discrimination between pathogen and host cells is due to electrostatic interactions between the cationic peptide and the negative phospholipids that form the external leaflet of the pathogen membrane, simulation showed that the lytic activity of these peptides must be preceded by a phospholipid segregation, without which the pathogen membrane would show a great mechanical stability. However, as a consequence of this phospholipid segregation (induced by the presence of charged peptides in the vicinity of the membrane), mechanical inhomogeneities emerge in the membrane, promoting the membrane rupture when a threshold concentration of peptides adsorbed on the membrane is achieved, in lipid patches with low concentrations of charged phospholipids. Thus, the existence of some patches in the membrane in which the insertion of peptides is more favourable than in others (from a thermodynamic point of view), together with the mechanical inhomogeneities associated to its lipid composition, seem to be a key factor in explaining the molecular activity of these small cationic peptides.

As regards the effect of the ionic strength on the inhibition of peptide activity, it was seen that an increase in the ionic strength of the aqueous solution increased the

stiffness and mechanical stability of the membrane (determined as an increase in the values of k^b), and the screening of peptide-membrane electrostatic interactions. As a consequence of both effects, an inhibition of antimicrobial activity is expected, which is in line with experimental results.

Hence, our findings suggest that the lytic effect of small cationic peptides should be considered as a dynamic picture of structural transformations adopted by the lipid-peptide mixture depending on the relative ratio of the two species, rather than a static picture of pores induced in the membrane by the presence of peptides.

6 Acknowledgements

This work was carried out without support from any National or Local Spanish Agency due to the cut in research funds for science. The authors wish to thank the Computing Center of the Universidad Politecnica de Cartagena for providing the computational resources required to perform all the heavy computational work. AG, RDP and RDE are members of the CONICET (National Research Council, Argentina).

References

[1] H. Boman, *Cell*, 1991, **65**, 205–207.

[2] H. Boman, *Rev. Immun.*, 1995, **13**, 61–92.

[3] G. Gudmundsson, B. Agerberth, J. Odeberg, T. Bergman, B. Olsson and R. Salcedo, *Eur. J. Biochem.*, 1996, **238**, 325–332.

[4] R. Hancock and D. Chapple, *Antimicrobial agents and chemotherapy*, 1999, **43**, 1317–1323.

[5] M. Zasloff, *Nature*, 2002, **415**, 389–395.

[6] R. E. W. Hancock, *Lancet*, 1997, **349**, 418–422.

[7] R. E. W. Hancock and A. Patrzykat, *Current Drug Targets - Infectious Disorders*, 2002, **2**, 79–83.

[8] M. van der Rest, A. Kamminga, A. Nakano, Y. Anraku, B. Poolman and W. Konings, *Microbiological Review*, 1995, **59**, 304–322.

[9] M. R. Yeaman and N. Y. Yount, *Pharmacological reviews*, 2003, **55**, 27–55.

[10] V. Teixeira, M. J. Feio and M. Bastos, *Progress in Lipid Research*, 2012, **51**, 149–177.

[11] H. Jenssen, P. Hamill and R. Hancock, *Clinical Microbiology Reviews*, 2006, **19**, 492–511.

[12] A. Garro, M. Olivella, J. Bombasaro, B. Lima, A. Tapia, G. Feresin, A. Perczel, C. Somlai, B. Penke, J. L. Cascales, A. Rodriguez and R. Enriz, *Chem. Biol. Drug. Des.*, 2013, **82**, 167–177.

[13] M. Dathe, H. Nikolenko, J. Meyer, M. Beyermann and M. Bienert, *FEBS LETTERS*, 2001, **501**, 146–150.

[14] K. Matsuzaki, *Biochimica et Biophysica Acta*, 1999, **1462**, 1–10.

[15] A. Garro, F. Garibotto, A. Rodriguez, M. Raimondi, S. Zacchino, A. Perczel, C. Somlai, B. Penke and R. Enriz, *Letters in Drug Design and Discovery*, 2011, **8**, 562–567.

[16] Y. Shai, *Trends in biochemical sciences*, 1995, **20**, 460–464.

[17] H. Huang, *Biochemistry*, 2000, **39**, 8347–8352.

[18] H. Berendsen, D. V. der Spoel and R. V. R, *Comput. Phys. Commun.*, 1995, **91**, 43–56.

[19] E. Lindahl, B. Hess and D. van der Spoel, *J. Mol. Modeling*, 2001, **7**, 306–317.

[20] T. Darden, D. York and L. Pedersen, *J. Chem. Phys.*, 1993, **98**, 10089–10092.

[21] U. Essmann, L. Perera, M. B. T. Darden, H. Lee and L. Pedersen, *J. Chem. Phys.*, 1995, **103**, 8577–8593.

[22] B. Jonsson, O. Edholm and O. Teleman, *Journal of Chemical Physics*, 1986, **85**, 2259–2271.

[23] E. Egberts, S. J. Marrink and H. J. C. Berendsen, *Eur. Biophys. J.*, 1994, **22**, 423–436.

[24] P. Ahlstrom and H. Berendsen, *Journal of Physical Chemistry*, 1993, **97**, 13691–13702.

[25] J. J. López Cascales, J. García de la Torre, S. Marrink and H. Berendsen, *J. Chem. Phys.*, 1996, **104**, 2713–2720.

[26] P. David, W. van Gunsteren and A. Mark, *Journal of Computational Chemistry*, 2010, **31**, 1117–1125.

[27] B. Hess, H. Bekker, H. Berendsen and H.J.C. Fraaije, *J. Comp. Chem.*, 1997, 1463–1472.

[28] H. J. C. Berendsen, J. P. M. Postma, W. F. van Gunsteren, A. DiNola and J. R. Haak, *J. Chem. Phys.*, 1984, **81**, 3684–3690.

[29] A. Seeling and J. Seeling, *Biochemistry*, 1974, **23**, 4839–4845.

[30] G. Cevc, A. Watts and D. Marsh, *Biochemistry*, 1981, **20**, 4955–4965.

[31] E. Luna and H. Mcconnell, *BBA*, 1977, **470**, 303–316.

[32] N. Schmid, A. Eichenberger, M. Winger, A. Mark and W. van Gunsteren, *Eur. Biophys. J.*, 2011, **7**, 843–856.

[33] H. J. C. Berendsen, J. P. M. Postma, W. F. van Gunsteren and J. Hermans, *Intermolecular Forces*, D. Reidel Publishing Company, 1981.

[34] M. Orsi, D. Haubertin, W. Sanderson and J. Essex, *J. Chem. Phys. B.*, 2008, **112**, 802–815.

[35] N. Chu, N. Kucerka, Y. Liu, S. Tristram-Nagle and J. Nagle, *Phys. Rev. E.*, 2005, **71**, 71.041904.

[36] E. Evans and W. Rawicz, *Physical Review Letters*, 1990, **64**, 2094–2097.

[37] W. Rawicz, K. Olbrich, T. McIntosh, D. Needham and E. Evans, *Biophys. J*, 2000, **79**, 328–339.

[38] J. Pan, S. Tristram-Nagle, N. Kucerka and J. Nagle, *Biophysical J.*, 2008, **94**, 117–124.

[39] H. Seto, N. Yamada, M. Nagao, M. Hishida and T. Takeda, *Eur. Phys. J. E.*, 2008, **26**, 217–223.

[40] H. Petrache, S. Tristram-Nagle, K. Gawrisch, D. Harries, V. Parseguian and J. Nagle, *Biophysical J.*, 2004, **86**, 1574–1586.

[41] M. Claessens, B. van Oort, F. Leermakers, F. Hoekstra and M. C. Stuart, *Biophysical J.*, 2004, **87**, 3882–3893.

[42] S. Pandit, D. Bostick and M. Berkowitz, *Biophysical Journal*, 2003, **84**, 3743.

[43] J. Sachs, H. Nanda, H. Petrache and T. Woolf, *Biophysical Journal*, 2004, **86**, 3772.

[44] R. Porasso and J. López Cascales, *Colloids and surfaces B: Biointerfaces*, 2009, 42–50.

[45] A. Seeling and J. Seeling, *Biochemistry*, 1974, **23**, 4839–4845.

[46] J. Browning and J. Seelig, *Biochemistry*, 1980, **19**, 1262–1270.

[47] S. J. Marrink and H. J. C. Berendsen, *J. Phys. Chem.*, 1994, **15**, 4155–4168.

[48] E. Lindahl and O. Edholm, *J. Chem. Phys.*, 2000, **113**, 3882–3893.

[49] G. Torrie and J. Valleau, *J. Comput. Phys.*, 1977, **23**, 187–199.

[50] S. Kumar, D. Bouzida, R. Swensen, P. Kollman and J. Rosemberg, *J. Comp. Chem.*, 1992, **13**, 1011–1021.

[51] A. Polyansky, P.E.Volynsky, A. Arseniew and R. Efremov, *J. Chem. Phys. B.*, 2009, **113**, 1120–1126.

[52] K. Lam, H.Wang, T. Siaw, M. Chapman, A. Waring, J. Kindt and K. Lee, *Biochimica et Biophysica Acta*, 2012, **1818**, 194–204.

[53] Y. Shai, *Biochimica et Biophysica Acta (BBA)*, 1999, **1462**, 55–70.

[54] R. E. W. Hancock and G. Diamond, *Trends in microbiology*, 2000, **8**, 402–410.

[55] R.Bals, X. Wang, Z. Wu, T. Freeman, V. Bafna, M. Zasloff and J. Wilson, *J. Clin. Investig.*, 1998, **102**, 874–880.

[56] M. Javadpour and M. Barkley, *Biochemistry*, 1997, **36**, 9540–9549.

[57] B. Skerlavaj, M. Scocchi, R. Gennaro, A. Risso and M. Zanetti, *Antimicrobial Agents and Chemotherapy*, 2001, **45**, 715–722.

[58] Y. Shai, *Biopolymers - Peptide Science Section*, 2002, **66**, 236–248.

List of Tables

List of Figures